

# Volumetric Reconstruction From Partial Views for Task-Oriented Grasping

Fujian Yan, Hui Li, and Hongsheng He\*

**Abstract**—Object affordance and volumetric information are essential in devising effective grasping strategies under task-specific constraints. This paper presents an approach for inferring suitable grasping strategies from limited partial views of an object. To achieve this, a recurrent generative adversarial network (R-GAN) was proposed by incorporating a recurrent generator with long short-term memory (LSTM) units for it to process a variable number of depth scans. To determine object affordances, the AffordPose knowledge dataset is utilized as prior knowledge. Affordance retrieving is defined by the volume similarity measured via Chamfer Distance and action similarities. A Proximal Policy Optimization (PPO) reinforcement learning model is further implemented to refine the retrieved grasp strategies for task-oriented grasping. The retrieved grasp strategies were evaluated on a dual-arm mobile manipulation robot with an overall grasping accuracy of 89% for four tasks: lift, handle grasp, wrap grasp, and press.

**Index Terms**—3D volumetric composition, task-oriented grasping, generative adversary network, and views adaptive model.

## I. INTRODUCTION

Traditional robotic manipulation is typically designed for repetitive tasks involving identical objects. However, with the increasing deployment of robots in human-centric environments, there is a growing need for these systems to exhibit greater flexibility and adaptability, particularly in grasping strategies for previously unseen objects. For instance, assistive robots assembling furniture, such as chairs, must adjust their grasp based on the unique geometry of each component. Humans naturally estimate an object’s volume to determine optimal grasp points to ensure a stable and secure hold. Emulating this capability in robots can enhance their dexterity and effectiveness in handling diverse objects. This paper aims to replicate human-like volume assessment in robotic manipulation to enable stable grasping of various objects with partial views.

To develop a reliable grasping strategy, physics-based analysis methods have been proposed [1], [2]. These approaches typically assume complete knowledge of object properties, an assumption that does not hold, where objects are often unfamiliar or previously unseen [3]. To obtain the physic attributes of objects like volume, a grasping plan based on

synthetic point clouds was introduced in [4]. However, this method relies on 2.5D point clouds with comprehensive sensor coverage, making it unsuitable for scenarios where only partial object views are available. Shape-completion-based approaches have been explored [5], but these methods do not account for task-specific grasping constraints. Integrating object affordances into grasp planning can enhance task-aware grasping strategies, improving adaptability in real-world applications.

The problem of 3D volumetric reconstruction is essential for deriving 3D models from 2D or 2.5D sensing data. It aims to reconstruct the 3D surfaces and fill in the unobserved volumes beneath those surfaces [6]. Unlike 3D reconstruction or 3D shape generation, which primarily focus on surface reconstruction, 3D volumetric reconstruction seeks to create complete models encompassing volumetric, shape, and dimensional information. Such comprehensive models are valuable in various applications, including robotic manipulation [7], object deformation [8], robotic scene understanding [9], and human-robot collaboration [10]. Traditional 3D reconstruction methods based on feature matching and view registration, such as structure from motion (SfM) [11] and visual simultaneous localization and mapping (SLAM) [12], usually require a large number of scans from different perspectives with dense features [13]. It is challenging for these methods to reconstruct a 3D model with limited scans. Due to the restricted point of view (POV) of an RGB-D sensor, it is often impractical to cover all surfaces with just a few scans. Consequently, the reconstructed 3D models may miss significant components. Hole-filling techniques, such as Laplacian hole filling [14] and Poisson surface reconstruction [15], can handle minor holes in the reconstructed models but face challenges in processing or generating complex structures.

In this paper, we proposed an approach for task-oriented grasping of unseen objects using constructed object volumes and affordance knowledge. To achieve this, we designed a recurrent generative adversarial (R-GAN) model to reconstruct object volumes from limited scans, akin to how humans reconstruct object volume from slight peaks. The R-GAN model learns a smooth function that maps depth scans to volumetric reconstructions. The model integrates a recurrent generator with a 3D convolutional encoder-decoder structure augmented by Long Short-Term Memory (LSTM) units. The encoder extracts features that represent stereoscopic structures from the depth scans and compresses them into

Fujian Yan is with the School of Computing, Wichita State University, Wichita, KS, 67260, USA

Hui Li and Hongsheng He are with the Department of Computer Science, The University of Alabama, Tuscaloosa, AL 35487 USA.

\*Correspondence should be addressed to Hongsheng He, hongsheng.he@ua.edu.

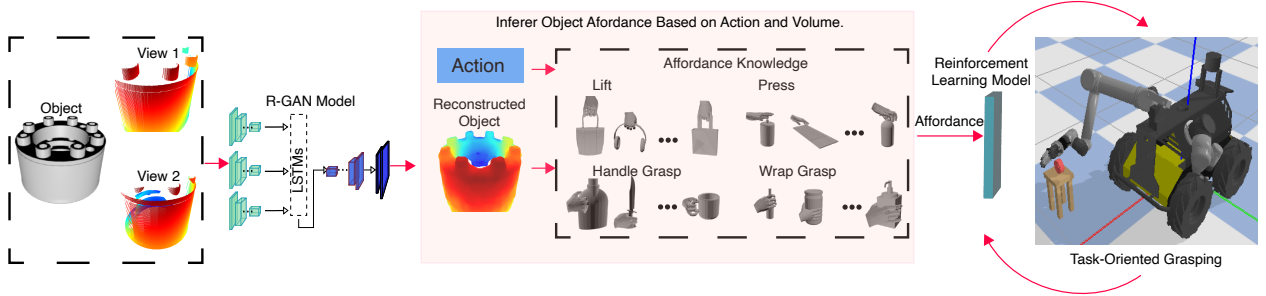


Fig. 1

TASK-ORIENTED GRASPING BASED ON VOLUMETRIC RECONSTRUCTION AND AFFORDANCE KNOWLEDGE.

a latent space. Leveraging LSTM’s memorization ability, the model can process a single or a sequential depth scans. The decoder, followed by LSTM units, decodes these features back into a 3D representation. The discriminator, composed of 3D convolutional layers, compares the reconstructed model with the object’s point cloud. To predict the optimal grasping strategy, we designed a grasping approximation model that takes the volume of objects as input, then computes the similarity against objects in AffordPose knowledge dataset, which is a large-scale dataset of task-oriented hand-object interactions with affordance-driven hand poses [16]. This knowledge base provides task-based grasp strategies informed by object affordances. The retrieved grasping strategy are refined by reinforcement learning approach [7], and the proposed approach was evaluated on a dual-arm robot.

The major contributions of the paper include: 1) The design of the R-GAN model for reconstructing volume of objects rather than just the 3D shape. 2) Enabling robots to learn volumetric knowledge of unseen objects.

## II. VOLUME RECONSTRUCTION FOR TASK-ORIENTED GRASPING

As illustrated in Fig. 1, the framework of task-oriented grasping based on volumetric reconstruction and affordance knowledge comprises three key components: volumetric reconstruction, affordance-based grasp inference, and reinforcement learning. Limited depth scans are collected to reconstruct the object’s volume. The action (e.g. lift, grasp) and the reconstructed volume are used to find similar objects in the affordance knowledge base to infer object affordance. As affordance decides the grasping pose for a task, it may not fit the real-world object accurately. A reinforcement learning model is therefore developed to refine the grasp for optimal grasping strategies.

While RGB-D sensors are widely employed for capturing depth information, a single RGB-D sensor provides depth data from only a single point of view (POV), limiting the ability to reconstruct a complete 3D model [17]. Although multiple RGB-D sensors can be utilized to capture depth information from different perspectives, practical constraints

often make panoramic scanning infeasible in real-world applications [18].

We designed a Recurrent Generative Adversarial Network (R-GAN) to generate a 3D volumetric model from a single or a limited sequence of depth scans. The model processes these scans through an encoder that extracts sequential features  $S_1, S_2, \dots, S_n$ , which are then fed into a LSTM layer for temporal feature learning. The encoder structure is dynamically adapted based on the number of available depth scans to ensure flexibility in different scanning scenarios. The proposed R-GAN model allows flexible integration of single or multiple depth scans, thereby enabling robust 3D object reconstruction under varying conditions.

### A. 3D Volumetric Reconstruction

The main challenge for 3D volumetric reconstruction is generating unknown points beneath the surface. To solve this problem, we extend the vanilla GAN model to compose unknown points. The recurrent generator in the R-GAN model can take sequential depth inputs to reconstruct 3D volumetric models  $\hat{Y}$ . The discriminator takes both  $\hat{Y}$  and ground truth  $Y$  as inputs to differentiate them.

The designed model can adaptively take a single depth scan or a few multiple depth scans  $\{X_i | X_i \in \mathbb{R}^{m \times m \times m}, i = 1, 2, 3, \dots, n\}$ . The model maps input data  $X_i$  to a latent space to approximate the volume. To get accurate 3D volumetric reconstruction, the model approximates parameters  $\theta_{\text{gen}}$  for the generator and  $\theta_{\text{dis}}$  for the discriminator by

$$\theta_{\text{gen}}^*, \theta_{\text{dis}}^* = \min_{\theta_{\text{gen}}} \max_{\theta_{\text{dis}}} (f_{\text{gen}}(\theta_{\text{gen}}, X_1, \dots, X_i), f_{\text{dis}}(\theta_{\text{dis}}, Y_j, f_{\text{gen}}(\cdot))) \quad (1)$$

where  $Y_j$  is the corresponding ground truth for a single depth scan  $X$  or multiple-views depth scans  $X_i$ .  $\theta_{\text{gen}}^*$  is optimized parameters for the generator, and  $\theta_{\text{dis}}^*$  is the optimized parameter for the discriminator. The model contains a generator  $f_{\text{gen}}(\cdot) : X_i \rightarrow \hat{Y}$  that reconstructs 3D volumetric model  $\hat{Y}$  from the inputs, and a discriminator  $f_{\text{dis}}(\cdot)$  to determine how different between the  $\hat{Y}$  and ground truth  $Y$ . Sequential

depth scans  $\{X_i | X_i \in \mathbb{R}^3, i = 1, 2, 3, \dots, n\}$  are taken by the generator

$$f_{\text{gen}} : \hat{Y} = \sigma \left( \sum_{i=1}^N \mathbf{W}_{\text{gen}}^i X_i + \mathbf{b}_{\text{gen}}^i \right) \quad (2)$$

where  $\mathbf{W}_{\text{gen}}^i$  and  $\mathbf{b}_{\text{gen}}^i$  are weights and bias for each encoder in the generator network, respectively. The  $i$  is the indicator for a specific number of the encoders for adaptively taking the input scans. To extract features from an input data, we designed an encoder that is constructed by a five-layer 3D convolutional neural network (3D-CNN).

The vanilla GAN model can take a single-depth scan of an object as input to approximate 3D volumetric information. However, when provided with multiple depth scans, it treats each scan as an independent input. To train the model with multiple depth scans, we extend the generator with LSTM units. To generate sequential inputs for LSTM units, each extracted feature tensor  $x_t$  from each encoder is flattened to  $\bar{x}_t^k$ , where  $k$  is the view index. The concatenated sequential tensor  $\mathbf{X}_t = \{\bar{x}_t^1, \bar{x}_t^2, \dots, \bar{x}_t^n\}$ , which has a dimension of  $(m \times t \times f)$ . The  $m$  is number of depth scans,  $t$  is the time-step, and  $f$  is the number of elements in each feature. The LSTM units in the proposed method consists of three gates governing data flow from the encoder to the decoder in the generator. The input gate  $i_t$  control the data flow from the input to the hidden state  $h_t$ , the forget gate  $f_t$  controls the data flow from previous hidden state  $h_{t-1}$  to current hidden state  $h_t$ , the operation of an LSTM unit can be described as

$$\begin{aligned} i_t &= \sigma(\mathbf{W}_i \cdot [\mathbf{X}_t, \mathbf{h}_{t-1}] + \mathbf{b}_i) \\ f_t &= \sigma(\mathbf{W}_f \cdot [\mathbf{X}_t, \mathbf{h}_{t-1}] + \mathbf{b}_f) \\ o_t &= \sigma(\mathbf{W}_o \cdot [\mathbf{X}_t, \mathbf{h}_{t-1}] + \mathbf{b}_o) \\ s_t &= f_t \odot s_{t-1} + i_t \odot \tanh(\mathbf{W}_s \cdot [\mathbf{X}_t, \mathbf{h}_{t-1}] + \mathbf{b}_s) \\ h_t &= o_t \odot \tanh(s_t) \end{aligned} \quad (3)$$

where  $\mathbf{W}_i, \mathbf{W}_f, \mathbf{W}_o, \mathbf{W}_s$  are weights for the input gate, the forget gate, the output gate, and the memory cell, respectively. The terms  $\mathbf{b}_i, \mathbf{b}_f, \mathbf{b}_o, \mathbf{b}_s$  are bias for the input gate, the forget gate, the output gate, and the memory cell, respectively. The memory cell is represented by  $s_t$ . We used  $\odot$  to represent element-wise multiplication.

The inputs  $X_i$  are fed into the 3D convolutional encoder with five 3D convolutional layers. In contrast to generators in vanilla GAN models, which generate data randomly. The recurrent generator in the designed model can generate data based on depth views. Two fully connected layers are used to flat these extracted features from the encoder to feed into the LSTM units. Also, these extracted features are sequentially concatenated. LSTM units are followed by a five layers 3D-CNN decoder and a two layers 3D-CNN up-scaling network.

The discriminator can evaluate the difference between the reconstructed 3D volumetric model  $\hat{Y} \in \mathbb{R}^{m \times m \times m}$  and the 3D CAD model (ground truth)  $Y \in \mathbb{R}^{m \times m \times m}$  of an object. The difference between the average output of the discriminator for the reconstruction model  $\hat{Y}$  and the ground truth  $Y$  is calculated by

$$m = \frac{1}{K} \sum_1^K f_{\text{dis}}(\hat{Y}) - \frac{1}{J} \sum_1^J f_{\text{dis}}(Y) \quad (4)$$

where  $K$  and  $J$  are the number of elements in  $f_{\text{dis}}(\hat{Y})$  and  $f_{\text{dis}}(Y)$  respectively. The term  $f_{\text{dis}}(\cdot)$  is a 3D-CNN contains six 3D convolutional layers, and the first five 3D convolutional layers are activated by ReLU and the last layer takes the sigmoid function as the activation function.

In order to train the model, we generate a substantial amount of training and testing data with artificially rendered depth scans of an object and its complete point cloud. Each object is placed in the Blender environment, and the ambient light and geometrical structures of the environment are the same. A synthetic RGB-D camera is placed in the environment and takes sequential depth scans of the object in the first and second quadrants in the x-y plane. The synthetic RGB-D camera is placed 1.6 meters away from the object. The resolution of each depth scan is  $512 \times 512$ .

### B. Task-Oriented Grasping with Knowledge of Object Affordance

Object affordance refers to the potential actions an object offers based on its shape, material, and function. The function defines the intended action (e.g., grasping, pouring), while the shape determines geometric compatibility with the manipulator. An object affords an action if its shape, size, and orientation align with task constraints. For example, a cup affords pouring due to its open top (task relevance) and graspable shape (volumetric match). In robotics, understanding affordance enables robots to interact with objects effectively, facilitating grasping and manipulation without explicit instructions.

Determining object affordance is challenging due to variations in design, context dependence, and ambiguity. Objects within the same category differ in shape, requiring generalization while ensuring precise interaction. Affordances also depend on orientation and environment, as a chair affords sitting only when upright. Ambiguous affordances, such as a screwdriver's multiple uses, further complicate decision-making.



Fig. 2

PART-LEVEL AFFORDANCES ARE ANNOTATED, AND THE CORRESPONDING GRASPING STRATEGY IS THEN MATCHED TO EACH AFFORDANCE.

In this paper, we infer object affordance from the AffordPose knowledge dataset [16], which provides part-level

affordance labeling and a corresponding grasping strategy, as shown in Fig. 2. The annotated grasp strategy specifies the grasp pose, along with the relative position and orientation between the hand and the object part, enabling more adaptive and informed robotic grasping.

To improve efficiency, the AffordPose dataset was reorganized into task categories (e.g., handle grasp, wrap grasp, lift, press). The framework first identified the task category  $c$  and then computed the volume similarity  $d'$ . The object with the smallest  $d'$  was selected for grasping strategy transfer

$$d' = \min_{O_i \in c} d_{\text{CD}}(O_r, O_i) \quad (5)$$

where  $O_r$  is the reconstructed object, and  $O_i$  is the  $i^{\text{th}}$  object under category  $c$ . The Chamfer Distance (CD),  $d_{\text{CD}}$ , is defined as

$$d_{\text{CD}}(O_r, O_i) = \sum_{p \in O_r} \min_{q \in O_i} \|p - q\|^2 + \sum_{q \in O_i} \min_{p \in O_r} \|q - p\|^2 \quad (6)$$

where  $p$  is a point in the reconstructed object's point cloud  $O_r$ , and  $q$  is a point in the reference object's point cloud  $O_i$ . The term  $\min_{q \in O_i} \|p - q\|^2$  finds the closest point in  $O_i$  for each point in  $O_r$ , while  $\min_{p \in O_r} \|q - p\|^2$  finds the closest point in  $O_r$  for each point in  $O_i$ . The summation aggregates these distances to quantify the overall shape difference.

The retrieved grasping strategy may not fit the reconstructed object well. To further adapt it to the reconstructed object and ensure stability, a Proximal Policy Optimization (PPO) reinforcement learning model from our previous work [7] was employed. The PPO model refines the retrieved grasping strategy by iteratively adjusting the grasp location and grasp pose to better conform to the reconstructed object's geometry and properties. For each grasping task, the robotic hand moves to the grasping point and executes the grasp. The action space includes the eight joints of the Schunk robotic hand, while the observation space comprises the relative pose, distance, and contact forces between the hand and the object. A binary reward function assigns 1 for successful grasps and 0 otherwise. Through continuous optimization, the model improves grasp robustness, ensuring a more stable and reliable interaction with diverse reconstructed objects.

### III. EXPERIMENT

We evaluated the proposed framework on a dual-arm robotic platform, measuring the grasping success rate to assess its effectiveness. The volumetric reconstruction performance was evaluated using computer-aided design (CAD) models of objects from TraceParts<sup>1</sup>, which contains comprehensive objects with precisely details.

#### A. Performance of 3D Volumetric Reconstruction

In order to appraise the R-GAN model, we performed three experiments: evaluation on AffordPose, evaluation on TraceParts, and comparison study with two other 3D volumetric reconstruction models.

<sup>1</sup><https://www.traceparts.com/en>

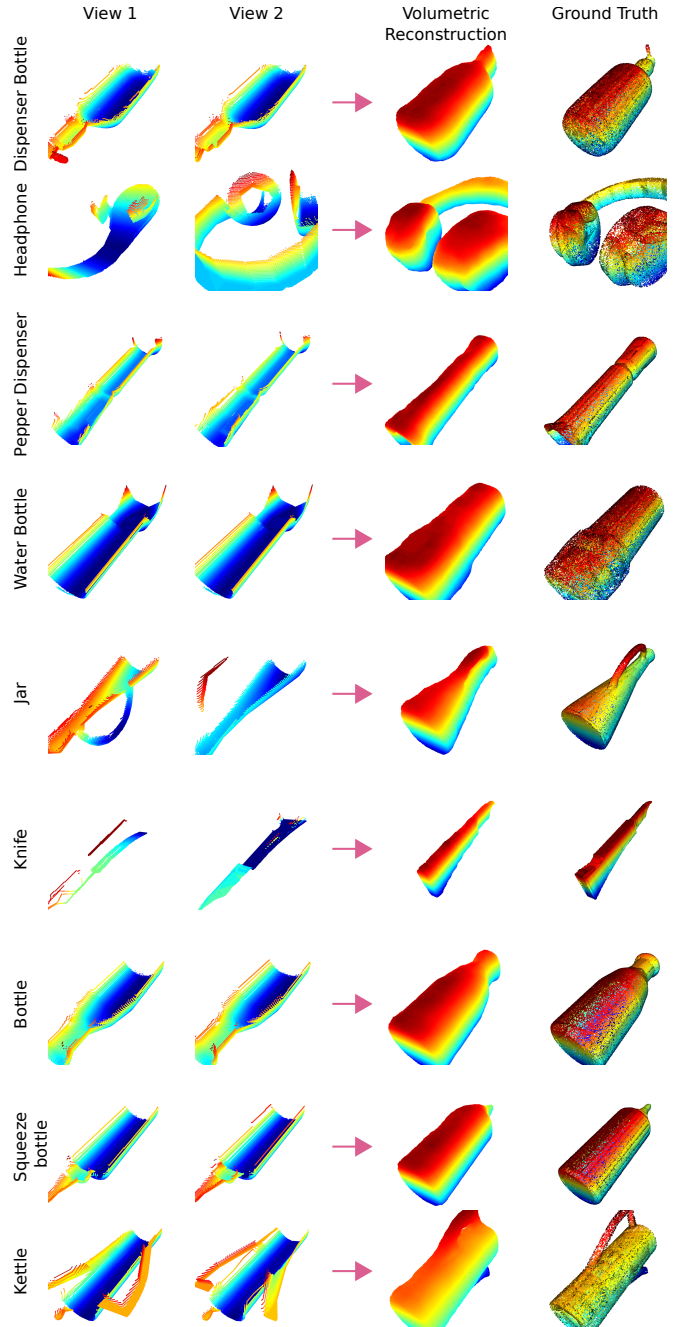


Fig. 3

VOLUMETRIC RECONSTRUCTION RESULTS OF AFFORDPOSE DATASET OBJECTS.

Volumetric reconstruction results of objects in the AffordPose database are shown in Fig. 3, and volumetric reconstruction results of objects in the dataset are shown in Fig. 4. Based on the results in Figs. 3 and 4, the proposed model can successfully reconstruct object volume based on the partial scans. The proposed model can reconstruct precise structures of objects such as nuzzle, curly handle, local hollow parts, and convex parts. However, minor details of

parts of the object, which are not included in-depth scans, are hard to reconstruct, as the discriminator neglected relatively smaller parts of an object. The absence of these small parts in reconstruction is a common layback of deep learning-based volumetric reconstruction methods.

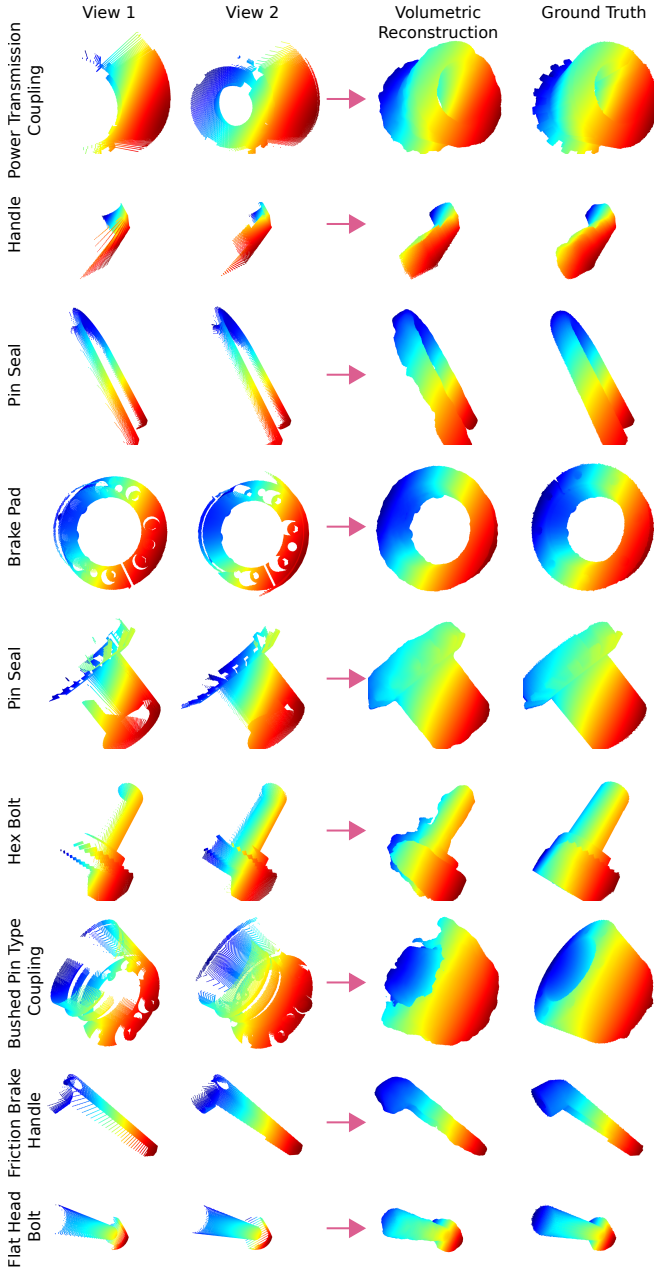


Fig. 4

VOLUMETRIC RECONSTRUCTION RESULTS OF OBJECTS IN THE STANDARD DATASET.

We computed and compared the mean of IoU, Hit-rate (HR), and Accuracy of each category shown in the Table I. The IoU was calculated between the 3D fulfilling models that were generated based on depth scans and CAD models. IoU

is computed as  $\text{IoU} = \frac{\sum_{i=0}^N y_i \cap \hat{y}_i}{\sum_{i=0}^N y_i \cup \hat{y}_i}$ , where  $y_i$  was the  $i_{\text{th}}$  voxel in the 3D fulfilling model, and the  $\hat{y}_i$  was the  $i_{\text{th}}$  voxel in the 3D CAD model. The hit-rate is the rate of the reconstructed models of the object that, in the region of the ground truths point clouds. It indicated how complete the reconstruction model is. The hit-rate is computed as  $\text{HR} = 1 - (\sum_{i=0}^N (y_i \cap \hat{y}_i) \oplus \hat{y}_i / \sum_{i=0}^N y_i \cup \hat{y}_i)$ . The accuracy showed how well the composed model is. It is computed as  $\text{Accuracy} = 1 - (\sum_{i=0}^N (y_i \cap \hat{y}_i) \oplus y_i / \sum_{i=0}^N y_i \cup \hat{y}_i)$ .

There were 125 depth scans were acquired from different angles for each object in each category in the Blender environment. HR can describe the completeness of the reconstructed parts in the 3D reconstruction models. In detail, the higher the HR results are, the more complete the volumetric reconstruction models are. Accuracy can describe the correctness of the 3D-composed results. The higher the accuracy is, the more points are correctly composed. The IoU, HR, and Accuracy for “Power transmission”, “Sealing”, and “Handles” of 3DR2N2 and single-view 3D reconstruction [9] methods are estimated, and they are marked with an asterisk (\*). The IoU, HR, and Accuracy of the proposed R-GAN model achieved 77.71%, 80.08%, and 97.45% on average. Based on the results shown in Table I, the proposed method outperformed other methods in IoU, HR, and Accuracy. Therefore, the results proved that for reconstructing 3D models, additional depth scans could achieve better reconstruction results.

Based on the results shown in Table I, volumetric reconstruction models in the “Sealing” category achieved the highest IoU, and volumetric reconstruction models in the “Fastener” category achieved the lowest IoU. The reason is that the structures of objects in the “Sealing” are relatively simple, are majorly ring-shaped, and without complex engraved lines. Objects in the “Fastener” category are not in the training dataset or the testing dataset, and their structures are relatively complex, like fillet conjunctions between rods and heads. Objects in the “Linear and rotary motion” and the “Power transmission” categories are both cylinder shapes. However, the accuracy for reconstructed 3D models in the “Linear and rotary motion” is 93.11%, and it is 6.54% lower than the accuracy for reconstructed 3D models in the “Power transmission” category. Objects in the “Linear and rotary motion” category are normally longer than objects in the “Power transmission” category. Therefore, the depth scans have larger missing parts than objects in the “Power transmission” category.

### B. Task-Oriented Grasping

To evaluate the performance of the proposed framework in task-oriented grasping, four objects were reconstructed and compared with 3D models from the revised AffordPose knowledge base. The grasping strategy of the most volume-similar object was applied. To improve efficiency, the AffordPose dataset was reorganized into four task categories: handle grasp, wrap grasp, lift, and press. The framework first

TABLE I  
COMPARISON RESULTS IN IOU, HR, AND ACCURACY.

| Category                 | IoU           |             |                 | Hit-Rate      |             |                 | Accuracy      |             |                 |
|--------------------------|---------------|-------------|-----------------|---------------|-------------|-----------------|---------------|-------------|-----------------|
|                          | This Paper    | 3DR2N2 [19] | Single-View [9] | This Paper    | 3DR2N2 [19] | Single-View [9] | This Paper    | 3DR2N2 [19] | Single-View [9] |
| Brake/clutch/coupling    | <b>79.9%</b>  | 64.2%       | 70.48%          | <b>81.01%</b> | 65.09%      | 71.46%          | <b>98.90%</b> | 64.2%       | 70.48%          |
| Linear and rotary motion | <b>81.87%</b> | 73.85%      | 76.46%          | <b>88.77%</b> | 73.85%      | 76.46%          | <b>93.11%</b> | 73.85%      | 76.46%          |
| Power transmission       | <b>76.31%</b> | 62.45%*     | 69.25%*         | <b>76.88%</b> | 69.53%*     | 67.75%*         | <b>99.65%</b> | 66.25%*     | 74.02%*         |
| Sealing                  | <b>83.77%</b> | 68.56%*     | 77.13%*         | <b>82.68%</b> | 60.22%*     | 72.86%*         | <b>99.88%</b> | 66.40%*     | 74.19%*         |
| Handles                  | <b>73.37%</b> | 60.05%*     | 67.06%*         | <b>76.76%</b> | 64.76%*     | 67.64%*         | <b>96.63%</b> | 64.24%*     | 71.78%*         |
| Fastener                 | <b>71.06%</b> | 53.3%       | 67.12%          | <b>74.56%</b> | 53.3%       | 67.12%          | <b>96.51%</b> | 53.3%       | 67.12%          |
| Average                  | <b>77.71%</b> | 57.1%       | 71.32%          | <b>80.08%</b> | 64.45%      | 70.55%          | <b>97.45%</b> | 64.71%      | 72.33%          |

identified the relevant task category, then computed volume similarity using the Chamfer Distance (CD). The object with the smallest CD was selected for grasping strategy transfer.

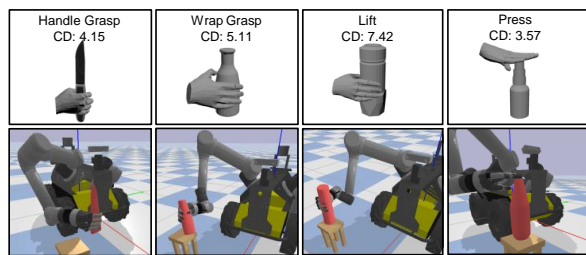


Fig. 5

TASK-ORIENTED GRASPING. THE FIRST ROW DISPLAYS THE MOST VOLUME-SIMILAR OBJECT FROM THE KNOWLEDGE BASE ALONG WITH ITS CORRESPONDING GRASP STRATEGY. THE SECOND ROW SHOWS THE GRASPING RESULTS FOR THE RECONSTRUCTED OBJECT.

Figure 5 presents the comparison and grasping results. Experiments showed that, within the same task, higher volume similarity generally led to a more similar grasping strategy. However, for different tasks, functional requirements played a more significant role in determining the appropriate grasp.

A comprehensive reinforcement learning model was trained to adapt the retrieved grasping strategy to the reconstructed object and ensure stability. For each grasping task, the model selected a grasping point within a predefined region centered on the retrieved grasping point ( $\pm 3$  cm tolerance). The robotic hand moved to the grasping point and executed the grasp. The action space included the eight joints of the Schunk robotic hand, while the observation space comprised relative pose, distance, and contact forces between the hand and the object. A binary reward function assigned 1 for successful grasps and 0 otherwise.



Fig. 6

EVALUATION RESULTS FOR THE COMPREHENSIVE REINFORCEMENT LEARNING MODEL. EACH GRASPING TASK WAS PERFORMED 100 TIMES, AND THE SUCCESS RATE WAS RECORDED.

The model was trained on the four objects over 1,000 episodes and evaluated in 100 trials, achieving an 89% testing success rate (Fig. 6). Analysis revealed that handle grasping and pressing had higher success rates. Pressing required only actuator movement, while handle grasping benefited from high volume similarity with the knowledge base, ensuring reliable grasping.

Conversely, lifting had lower success rates due to the reconstructed object's larger size, resulting in a higher CD and reduced grasp stability. Wrap grasping also performed poorly due to missing fine details in reconstruction, such as the bottleneck, leading to slipping during execution.

#### IV. CONCLUSION

This paper presents a task-oriented grasping framework that integrates both volumetric and affordance knowledge. The proposed R-GAN model reconstructs 3D object volumes from limited depth scans, leveraging LSTM units for sequential learning. By retrieving grasping strategies from the AffordPose dataset and refining them with PPO, the framework adapts to unseen objects. Experimental results demonstrate superior reconstruction accuracy and grasping performance compared to existing methods. The success rate achieved an average of 89% over 400 grasping tasks.

## REFERENCES

- [1] A. Rodriguez, M. T. Mason, and S. Ferry, "From caging to grasping," *The International Journal of Robotics Research*, vol. 31, no. 7, pp. 886–900, 2012.
- [2] J. Weisz and P. K. Allen, "Pose error robust grasping from contact wrench space metrics," in *2012 IEEE international conference on robotics and automation*. IEEE, 2012, pp. 557–562.
- [3] C. Goldfeder and P. K. Allen, "Data-driven grasping," *Autonomous Robots*, vol. 31, no. 1, pp. 1–20, 2011.
- [4] J. Mahler, J. Liang, S. Niyaz, M. Laskey, R. Doan, X. Liu, J. A. Ojea, and K. Goldberg, "Dex-net 2.0: Deep learning to plan robust grasps with synthetic point clouds and analytic grasp metrics," *arXiv preprint arXiv:1703.09312*, 2017.
- [5] J. Varley, C. DeChant, A. Richardson, J. Ruales, and P. Allen, "Shape completion enabled robotic grasping," in *2017 IEEE/RSJ international conference on intelligent robots and systems (IROS)*. IEEE, 2017, pp. 2442–2447.
- [6] M. Runz, K. Li, M. Tang, L. Ma, C. Kong, T. Schmidt, I. Reid, L. Agapito, J. Straub, S. Lovegrove *et al.*, "Frodo: From detections to 3d objects," in *Proceedings of the IEEE/CVF Conference on Computer Vision and Pattern Recognition*, 2020, pp. 14 720–14 729.
- [7] H. Li, Y. Zhang, Y. Li, and H. He, "Learning task-oriented dexterous grasping from human knowledge," in *2021 IEEE International Conference on Robotics and Automation (ICRA)*. IEEE, 2021, pp. 6192–6198.
- [8] H. Yin, A. Varava, and D. Kragic, "Modeling, learning, perception, and control methods for deformable object manipulation," *Science Robotics*, vol. 6, no. 54, p. eabd8803, 2021.
- [9] F. Yan, D. Wang, and H. He, "Comprehension of spatial constraints by neural logic learning from a single rgb-d scan," in *2021 IEEE/RSJ International Conference on Intelligent Robots and Systems (IROS)*, 2021, pp. 9008–9013.
- [10] S. A. Green, M. Billingham, X. Chen, and J. G. Chase, "Human-robot collaboration: A literature review and augmented reality approach in design," *International journal of advanced robotic systems*, vol. 5, no. 1, p. 1, 2008.
- [11] G. Yi, L. Jianxin, Q. Hangping, and W. Bo, "Survey of structure from motion," in *Proceedings of 2014 International Conference on Cloud Computing and Internet of Things*. IEEE, 2014, pp. 72–76.
- [12] G. Silveira, E. Malis, and P. Rives, "An efficient direct approach to visual slam," *IEEE transactions on robotics*, vol. 24, no. 5, pp. 969–979, 2008.
- [13] M. Nießner, M. Zollhöfer, S. Izadi, and M. Stamminger, "Real-time 3d reconstruction at scale using voxel hashing," *ACM Trans. Graph.*, vol. 32, no. 6, nov 2013. [Online]. Available: <https://doi.org/10.1145/2508363.2508374>
- [14] O. Sorkine, D. Cohen-Or, Y. Lipman, M. Alexa, C. Rössl, and H.-P. Seidel, "Laplacian surface editing," in *Proceedings of the 2004 Eurographics/ACM SIGGRAPH symposium on Geometry processing*, 2004, pp. 175–184.
- [15] M. Kazhdan, M. Bolitho, and H. Hoppe, "Poisson surface reconstruction," in *Proceedings of the fourth Eurographics symposium on Geometry processing*, vol. 7, 2006.
- [16] J. Jian, X. Liu, M. Li, R. Hu, and J. Liu, "Affordpose: A large-scale dataset of hand-object interactions with affordance-driven hand pose," in *Proceedings of the IEEE/CVF International Conference on Computer Vision (ICCV)*, October 2023, pp. 14 713–14 724.
- [17] K. Wang, G. Zhang, and H. Bao, "Robust 3d reconstruction with an rgb-d camera," *IEEE Transactions on Image Processing*, vol. 23, no. 11, pp. 4893–4906, 2014.
- [18] W. Wang, K. Yamakawa, K. Hiroi, K. Kaji, and N. Kawaguchi, "A mobile system for 3d indoor mapping using lidar and panoramic camera," in *Adjunct Proceedings of the 2015 ACM International Joint Conference on Pervasive and Ubiquitous Computing and Proceedings of the 2015 ACM International Symposium on Wearable Computers*, 2015, pp. 337–340.
- [19] C. B. Choy, D. Xu, J. Gwak, K. Chen, and S. Savarese, "3d-r2n2: A unified approach for single and multi-view 3d object reconstruction," in *European conference on computer vision*. Springer, 2016, pp. 628–644.